scientific reports

Check for updates

OPEN

Stretch strain shifts optic nerve head astrocyte metabolism to enrich α-ketoglutarate and the pentose phosphate pathway

Usa Suwannasual[1], Katherine R. Smart[2], Olivia Young[1], Eul Hyun Suh[1], Teresa D. Golden[2] & Denise M. Inman[1]✉

Optic nerve head (ONH) astrocyte deformation contributes to glaucoma pathology by increasing extracellular matrix (ECM) deposition which promotes fibrosis in the ONH. To investigate how fibrosis and effector Yes-associated protein (YAP) activation is linked to metabolism, we examined YAP and alteration of tricarboxylic acid (TCA) cycle intermediates. Rat ONH astrocytes were subjected to biaxial stretch at 1 Hz for 24 h while cultured on various substrates. Stretched ONH astrocytes provided with uniformly-labeled ^{13}C glucose ([U-$^{13}C_6$]glucose) for 2 h yielded TCA cycle metabolites identified using GC-MS. Nuclear YAP translocation, glucose transporter 1 (GLUT1), and the laminin receptor Integrin β4 were significantly increased when ONH astrocytes exposed to stretch strain were cultured on laminin. Global disruption of TCA cycle intermediates occurred in the stretched ONH astrocytes, with reductions of citrate, pyruvate, lactate and glutamine. Significantly elevated α-ketoglutarate (α-KG) derived from [U-$^{13}C_6$]glucose was observed in the stretched ONH astrocytes, concomitant with increased histone demethylation. Increases in specific isotopologues of α-KG derived [2,3-$^{13}C_2$]glucose as well as increased pentose phosphate pathway (PPP) enzymes, with decreased pyruvate and lactate, support shunting of glucose-6-phosphate into the PPP. Our findings suggest YAP is an important integrator of ECM changes that contributes to metabolic reprogramming in ONH astrocytes under glaucoma-associated stress.

Keywords YAP, Stable isotope tracing, Fibrosis, Laminin, Metabolic reprogramming

Elevated intraocular pressure observed in glaucoma results in the dysfunction and eventual death of retinal ganglion cells and the degeneration of the optic nerve[1]. Increasing evidence has shown that energy production is altered in the glaucomatous retina and optic nerve, resulting in metabolic deficits[2,3] and death of retinal ganglion cells (RGC). RGCs obtain essential cofactors or energy substrates from vasculature as well as neighboring cells, including astrocytes, the primary glial cell in the nerve fiber layer of the retina and the ONH[4]. ONH astrocyte processes wrap fasciculating RGC axons[5], thereby behaving as an important intermediary for energy substrate transfer between the vasculature and RGC axons. Evidence for transfer of lactate from astrocytes[6] or oligodendrocytes[7,8] to axons has been demonstrated in the optic nerve, and monocarboxylate and glucose transporters are abundant on axons traversing the ONH[9,10]. These observations lend weight to the potential for astrocytes in the ONH to provide lactate and glucose to axons to maintain their energetic demands, though this has not been directly demonstrated. In glaucoma, the metabolic unit consisting of neurons, glial cells, and blood vessels can be disrupted[11]. For example, increased glycolysis observed in glaucomatous optic nerve was accompanied by limits of the nerve to respond appropriately to increased energy demand[2] suggesting that under conditions of glaucoma, glia may fail to provide energy substrate to RGC axons. Fortuitously, decreased glycolysis in the glaucomatous retina could be mitigated by provision of pyruvate, bypassing glycolysis to provide carbon to the TCA cycle[12].

Astrocytes, a type of glial cell found throughout the central nervous system, play a crucial role in maintaining metabolic support to the ONH[13]. Elevated intraocular pressure (IOP) results in mechanical stress in the ONH

[1]Department of Pharmaceutical Sciences, North Texas Eye Research Institute, University of North Texas Health Science Center, Fort Worth, TX, USA. [2]Department of Chemistry, University of North Texas, Denton, TX, USA. ✉email: denise.inman@unthsc.edu

region, leading to optic cupping from the loss of RGC axons[14,15]. Multiple studies have demonstrated an association between mechanical stress and alterations in metabolism[16–19]. For example, ONH astrocytes exposed to stretch strain that mimics the frequency and stretch of those forces in the human ONH[20] increase their utilization of glycolysis to meet heightened energy demands[18].

The ONH contains a specialized ECM including several types of collagens, laminin, elastin, and fibronectin[21,22]. Collagen is found in the lamina cribrosa (LC) and the trabecular meshwork[23], while ONH astrocytes subjected to glaucoma-like conditions can synthesize elastin and fibronectin[24,25]. Additionally, laminin has been observed around optic nerve astrocytes[26]. The ECM in the ONH plays a role in supporting the integrity and metabolism of optic nerve axons and RGC[27] Elevation of IOP results in an increased ECM stiffness that initiates a feedback loop augmenting changes in the composition of ECM by promoting the synthesis and accumulation of ECM proteins[28,29]. This process can significantly alter the LC, resulting in ECM deposition and remodeling including altered biomechanical properties[28,30] initiated by transforming growth factor-β (TGF-β), bone morphogenic proteins (BMPs), and Wnt binding to plasma membrane receptors that activate the Smad and b-catenin signaling pathways[31]. Included in these intracellular cascades is the Hippo signaling pathway which responds to mechanical stimuli and contributes to regulation of proliferation, apoptosis, and metabolic control[32].

YAP (Yes-associated protein) and TAZ (Transcriptional coactivator with PDZ-binding motif) are transcriptional coactivators associated with the Hippo signaling pathway regulating cellular homeostasis[33]. Cells responding to ECM stiffness activate YAP through mechanical signals that result in its translocation to nucleus, altering cellular metabolism. YAP behaves as a mechanosensor to regulate cellular metabolism in immune cells and cancer cells by promoting glycolysis, lipogenesis and glutaminolysis[34–36]. ECM mechanosensing can activate YAP and TAZ proteins through ECM stiffening and stretching[37,38]. Focal adhesions and integrins serve as cellular mechanosensory elements responding to the ECM milieu, regulating YAP activity[39]. Activation of YAP induced enhanced expression of profibrotic genes in lamina cribrosa cells from glaucoma patients[40]. In addition to ECM stiffness, YAP is critical to the TGF-β1-induced fibrosis from Müller glia in diabetic rat retina[35]. The importance of YAP for metabolic reprogramming and fibrosis has been well-established in the context of cancer, so the interplay between ECM mechanosensing and YAP activity that may promote metabolic shifts in ONH astrocytes remains a worthwhile investigation. Our abiding interest is in how cellular metabolic response could reveal new avenues for glaucoma treatment. To that end, in the present study, we cultured rat ONH astrocytes on various ECM substrates and exposed them to mechanical stretch to determine whether we would observe differential YAP nuclear translocation and altered metabolism. We employed Gas Chromatography-Mass Spectrometry (GC-MS)-based [U-$^{13}C_6$] or [2,3-$^{13}C_2$]glucose stable isotope tracing to map glucose fate associated with TCA cycle and PPP in these cells. Applying this approach allows us to understand the metabolic implications of ECM alterations in the ONH.

Results

ECM substrate impacts YAP nuclear translocation in stretched ONH astrocytes

As a transcriptional coactivator, YAP needs to translocate to the nucleus in order to perform its role in modulating gene expression for multiple cell processes and metabolism[41]. To examine YAP nuclear translocation in ONH astrocytes under glaucoma-like conditions, we cultured ONH astrocytes on various ECM substrates chosen based on their presence in the human ONH, including collagen I, elastin, laminin, and pronectin; pronectin is an 980 amino acid artificial protein that contains a repeated peptide (GAAVTGRGDSPASAAGY) from fibronectin[42]. ONH astrocytes cultured on these various substrates were subjected to stretch strain (12% biaxial stretch at 1 Hz, see Methods). Immunofluorescence labeling using an antibody directed against YAP showed that YAP translocated to the nucleus upon stretch strain primarily in cells cultured on laminin and pronectin (Fig. 1A, white arrows). YAP nuclear translocation remained unchanged in stretched ONH astrocytes cultured on collagen I and elastin (Fig. 1B and C). Quantifying the proportion of cells exhibiting nuclear translocation of YAP confirmed the immunofluorescence, with stretched ONH astrocytes cultured on laminin and pronectin showing a significantly greater proportion of nuclear YAP compared to control ONH astrocytes (no stretching) (Fig. 1D and E).

GLUT1 and *Itgβ* 4 upregulated in stretched ONH astrocytes cultured on Laminin

Translocation of YAP results in alterations of cell metabolism including upregulation of glucose transporters and increased glycolytic activity[43]. Therefore, we determined whether mechanical stretch stimulation could upregulate the GLUT1 in ONH astrocytes (Fig. 2A-D). The greatest YAP translocation was observed for stretched ONH astrocytes cultured on laminin (Fig. 1D), so we focused the remainder of our investigation on ONH astrocytes cultured on laminin. Optical density analysis of immunolabeled cells showed that GLUT1 expression was significantly enhanced exclusively in stretch exposed-ONH astrocytes grown on laminin (Fig. 2B, D, E). GLUT1 expression did not increase significantly in ONH astrocytes grown on collagen-I, elastin, or pronectin (Supplementary Figure S1). YAP is considered an effector for integration of mechanical deformation[44] likely through plasma membrane receptors such as the integrins, which are particularly abundant in the ONH[45]. YAP activation has been shown to be correlated with integrin-β4 expression[46]. Therefore, we analyzed *Itgβ4* expression in ONH astrocytes cultured on laminin and found significantly upregulated *Itgβ4* expression in stretched ONH astrocytes (Fig. 2F). These results imply that enhanced *Itgβ4* expression might promote YAP activation, leading to increased GLUT1 expression in stretched ONH astrocytes cultured on laminin.

Mechanical stretch disturbed glycolysis and TCA cycle metabolites in ONH astrocytes

To obtain a detailed profile of metabolites in stretched ONH astrocytes cultured on laminin, the cells were extracted and analyzed by GC-MS. Heat map visualization of the normalized concentration of 14 metabolites across control (left) and stretch (right) ONH astrocytes cultured on laminin is shown in Fig. 3A; details for all

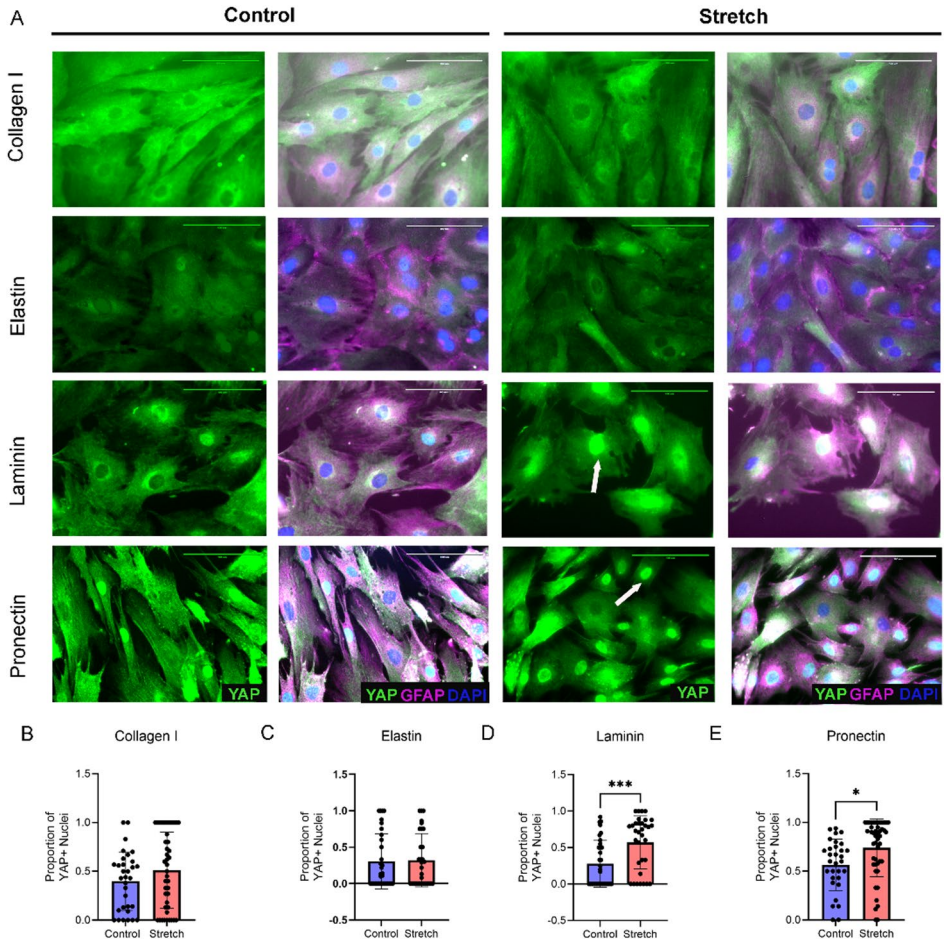

Fig. 1. Culture substrate impacts YAP translocation in stretched ONH astrocytes. **(A)** Immuno-fluorescence labeling with antibodies against YAP (green), GFAP (magenta) and nuclear stain DAPI (blue) showed YAP nuclear translocation after cells were exposed to 12% biaxial mechanical stretch at 1 Hz for 24 h compared to control cells not exposed to stretch. White arrows point to examples of YAP immunolabeling in the nucleus. Scale bar, 100 µm. The proportion of nuclei containing YAP immunolabel was quantified for cells cultured on **(B)** collagen I, **(C)** elastin, **(D)** laminin, or **(E)** pronectin. Data points represent fields of view taken from three independent biological replicates. The proportion of nuclear YAP was significantly increased for cells cultured on (D) laminin ($p < 0.001$) and (E) pronectin ($p < 0.05$). Data are mean ± SD and a two-way AVOVA with mixed-effects model was used for analysis. * $p < 0.05$, *** $p < 0.001$.

normalized metabolites are shown in Supplementary Figure S2. MetaboAnalyst 6.0 based t-test analysis identified significantly altered metabolites. Pyruvate and lactate, endproducts of glycolysis, were significantly decreased in stretched ONH astrocytes compared to control (Fig. 3B and C). Concordantly, levels of TCA cycle metabolites, including citrate and glutamine (Fig. 3D and E) were significantly decreased in stretched ONH astrocytes. In keeping with the reputation of astrocytes for being glycolytic and providing other cells such as neurons with lactate via extracellular transport, we reasoned that lactate levels could be reduced as a result of monocarboxylate transporter activity, so we examined extracellular lactate levels. However, stretched ONH astrocytes showed significantly decreased extracellular lactate as compared to control (Fig. 3F). Additionally, the expression of *Slc16a3* mRNA which encodes monocarboxylate transporter 4 (MCT4), a glial lactate exporter, was not changed in the stretch group compared to the control, suggesting altered extracellular lactate was independent of lactate transporter levels (Fig. 3G). The rest of the analyzed TCA cycle intermediates, including α-KG, succinate, fumarate, malate, and aspartate; and amino acids including leucine, lysine, phenylalanine, serine and valine did not differ between control and stretch conditions (Supplementary Figure S3). Overall, these results suggest that decreased glycolytic metabolites represent the feeding of these metabolites into the TCA cycle, allowing TCA cycle metabolites with the exception of citrate, to be maintained.

Stretched ONH astrocytes exhibited altered PPP enzyme expression

The reduced intracellular pyruvate and lactate in the stretched astrocytes cultured on laminin (Fig. 3B and C) suggest that glycolysis may be suppressed. Shunting of glucose-6-phosphate to the pentose phosphate or serine synthesis pathways (Fig. 4A) can result in an overall suppression of glycolysis, so we examined that possibility via quantitative PCR analysis for enzymes associated with the PPP including glucose-6-phosphate dehydrogenase

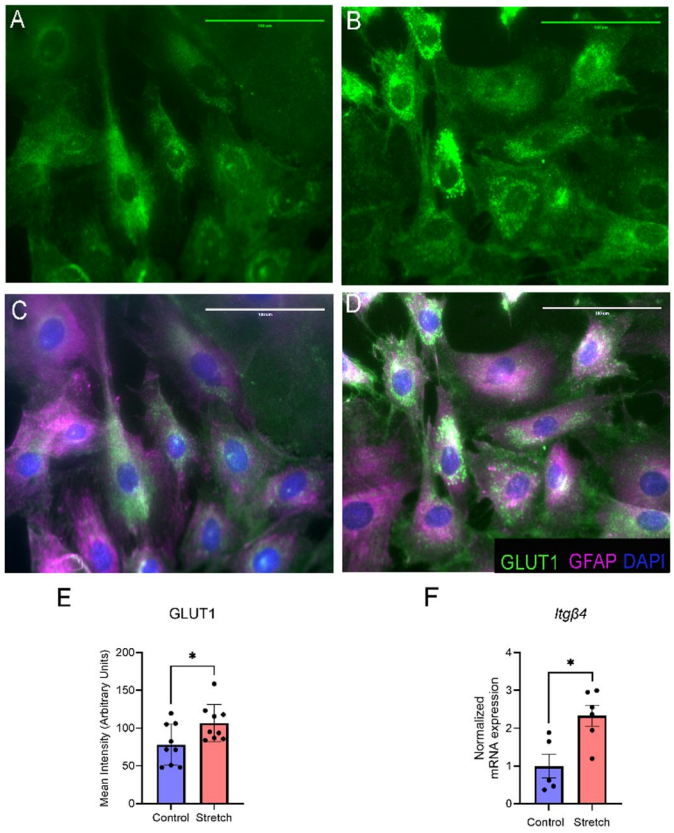

Fig. 2. YAP translocation accompanied GLUT1 and Itgb4 upregulation. Immunolabeling for GLUT1 (green) in **(A)** control ONH astrocytes and **(B)** stretched ONH astrocytes cultured on laminin. Panels **C** and **D** show GLUT1 (green) merged with GFAP (magenta) and counter-stained nuclei with DAPI (blue). GLUT1 expression in control (**A** and **C**) and stretch-exposed groups (**B** and **D**) was quantified in **(E)**, showing significantly increased GLUT1 expression as measured by mean intensity analysis in stretched ONH astrocytes ($p < 0.05$). Values in **(E)** are fields taken from across three independent biological replicates. Fields were $200 \times 280 \mu m^2$, with four fields examined per well from the central $1 cm^2$ of well area. Scale bar = 100 µm, 40× magnification. **(F)** Integrin-β4 (*Itgβ4*) mRNA expression showed significantly greater fold change in stretched ONH astrocytes ($p < 0.05$). Data were mean ± SD from a two-way AVOVA with mixed-effects model. * $p < 0.05$.

(*G6pd*), 6-phosphogluconate dehydrogenase (*6Gpd)*, and ribose-5-phosphate isomerase (*Rpi)* (Fig. 4B-D); and those associated with the serine synthesis pathway (SSP), including phosphoglycerate dehydrogenase (*Phgdh*), phosphoserine aminotransferase 1 (*Psat1*), and phosphoserine phosphatase (*Psph*) (Fig. 4E-G). The first enzyme in the PPP, *G6pd*, important for its production of NADPH, showed no difference between control and stretch mRNA expression (Fig. 4B). Further along in the PPP and important for ribose production, *6Gpd* mRNA expression was significantly upregulated in stretched ONH astrocytes (Fig. 4C). Taken together, these findings suggest a potential shunt of glycolytic intermediates into the PPP. However, mRNA expression of *Rpi* transcript levels were unchanged relative to control cells (Fig. 4D), and expression of SSP enzymes was likewise unaltered in stretched astrocytes (Fig. 4E-G). To further investigate whether glycolytic intermediates were being shunted into the PPP, we employed stable isotope tracing with [2,3-$^{13}C_2$]glucose which generates distinct isotopomer labeling patterns when metabolized via the PPP compared to glycolysis (Fig. 5A and Supplementary Figure S4 A and B). Tracing with [2,3-$^{13}C_2$]glucose enables distinction between glycolytic and PPP flux, as direct glycolysis generates [1,2-$^{13}C_2$]pyruvate/lactate, whereas metabolism through the oxidative PPP followed by re-entry into glycolysis yields [2,3-$^{13}C_2$]pyruvate/lactate[47]. These distinct labeling routes propagate into the TCA cycle, resulting in different isotopologue patterns and mass distributions in α-KG (Fig. 5A and Supplementary Figure S4). ONH astrocytes cultured on laminin were then cultured with [2,3-$^{13}C_2$]glucose to assess the mass isotopologue distribution (MID) of α-KG and to trace the metabolic fates of the labeled carbons through both glycolysis and the PPP. The results are shown in Fig. 5A. We found that α-KG (M + 1) or (M + 2), products of glycolysis, remained unchanged (Supplementary Figure S4C and D). PPP-associated α-ketoglutarate (M + 0), (M + 3) or (M + 5) did not show increased levels under stretch conditions (Fig. 5B-C, E). However, a small but significant increase in PPP-associated α-KG (M + 4) was detected in ONH astrocytes exposed to stretch strain (Fig. 5D). Taken together, these results suggest that glycolytic flux in stretched ONH astrocytes was affected by the diversion of glucose-6-phosphate into the PPP.

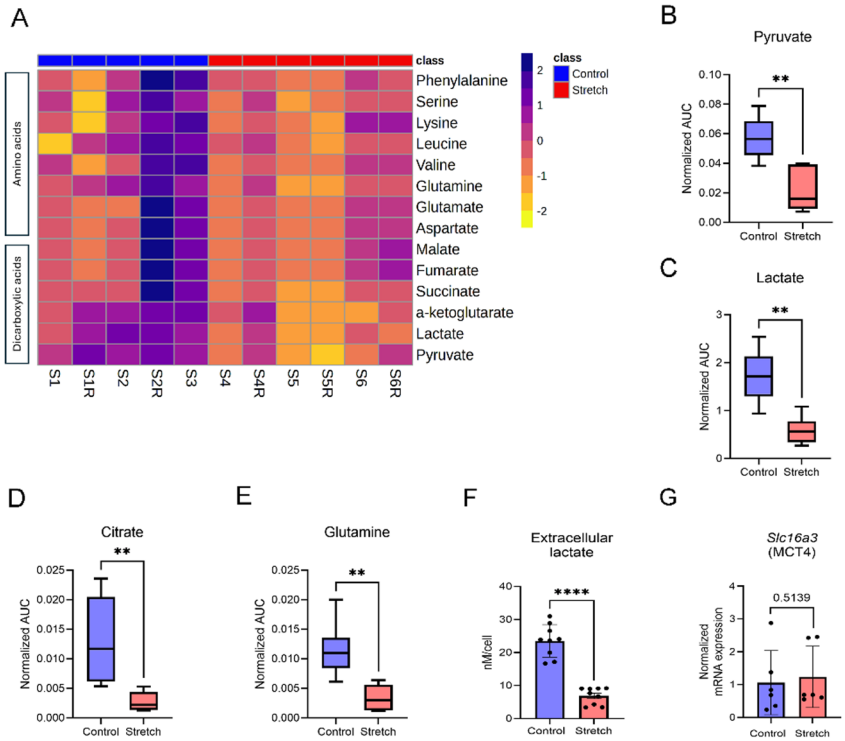

Fig. 3. Selected Glycolytic and TCA Cycle metabolites were significantly decreased in stretched ONH astrocytes. **(A)** Heat map showing the relative abundance of various metabolites, with color intensity indicating the Z-score corresponding to metabolite deviation from the mean. Data are from three biological replicates, with 2 technical replicates for each control and stretched sample shown; for example, S1 is the sample, and S1R is the technical replicate for the first Control sample. **(B)** Pyruvate levels were significantly reduced in stretched ONH astrocytes cultured on laminin ($p < 0.01$). **(C-E)** Similarly, lactate ($p < 0.01$), citrate ($p < 0.01$), and glutamine ($p < 0.01$) were all significantly decreased in stretched ONH astrocytes compared with controls. **(F)** Extracellular lactate levels in conditioned media from ONH astrocytes were significantly reduced in stretched cells compared with controls ($p < 0.0001$). Lactate concentrations (nM) were normalized to cell number which was determined just prior to lactate measurement. **(G)** Slc16a3 mRNA (monocarboxylate transporter 4; MCT4) expression was unchanged in stretched ONH astrocytes compared to control. A two-way AVOVA with mixed-effects model was used for analysis. Statistical significance is indicated as $^{**}p < 0.01$ and $^{****}p < 0.0001$.

Mechanical stretch altered PKM2 and PDH in ONH astrocytes

Our findings suggest that PPP was promoted in stretched ONH astrocytes, and we chose to confirm this finding by examining the rest of the glycolysis pathway (Fig. 6A). We measured hexokinase1 (HK 1) protein (Fig. 6B) and found that it was unchanged from control in stretched ONH astrocytes. We then analyzed the mRNA or protein of rate limiting enzymes of glycolysis including mRNA for pyruvate kinase M2 (*Pkm2*) and pyruvate dehydrogenase E1 (*Pdhe1*), and pyruvate dehydrogenase (PDH) protein. Stretched ONH astrocytes exhibited significantly higher *Pkm2* mRNA expression than did control cells (Fig. 6C). *Pdhe1* did not differ between stretched cells and control cells (Fig. 6D), nor did PDH protein (Fig. 6E). Additionally, mRNA expression of pyruvate carboxylase (PC) under stretch was significantly higher than to the control group (Fig. 6F), while the protein expression was unchanged (Fig. 6G). Taken together, it is possible *Pkm2* upregulation and PDH downregulation might be an attempt to boost pyruvate levels in the stretched ONH astrocytes since these alterations should contribute to the pyruvate pool.

Stable isotope tracing showed enrichment of α-ketoglutarate in stretched ONH astrocytes

Increased YAP nuclear translocation and GLUT1 expression in stretched astrocytes cultured on laminin (Fig. 2) prompted us to investigate the metabolic fate of glucose. The schematic in Fig. 7A shows the expected distribution of ^{13}C-labeled carbon in the first round of the TCA cycle after exposure to mechanical strain for 24 h and treatment of ONH astrocytes with [U-$^{13}C_6$]glucose and stretching for 2 h (Fig. 7B). Relative enrichment of glucose-derived labeled α-KG (M + 2) was significantly higher in stretched astrocytes than control cells (Fig. 7C). As a result of the potential exchange of α-KG with the glutamate-glutamine cycle in astrocytes, we evaluated extracellular glutamate, finding that extracellular ^{13}C-labeled glucose-derived glutamate (M + 2) was unchanged in stretched astrocytes (Fig. 7D). Importantly, the protein expression of high-affinity glutamate transporters EAAT 1 and EAAT 2 did not differ between stretched ONH astrocytes and control cells (Fig. 7E and F). These findings suggest that mechanical stretch on laminin promoted intracellular α-KG accumulation without suppression of release of glutamate in astrocytes, and no alteration of glutamate transporters. In addition, our

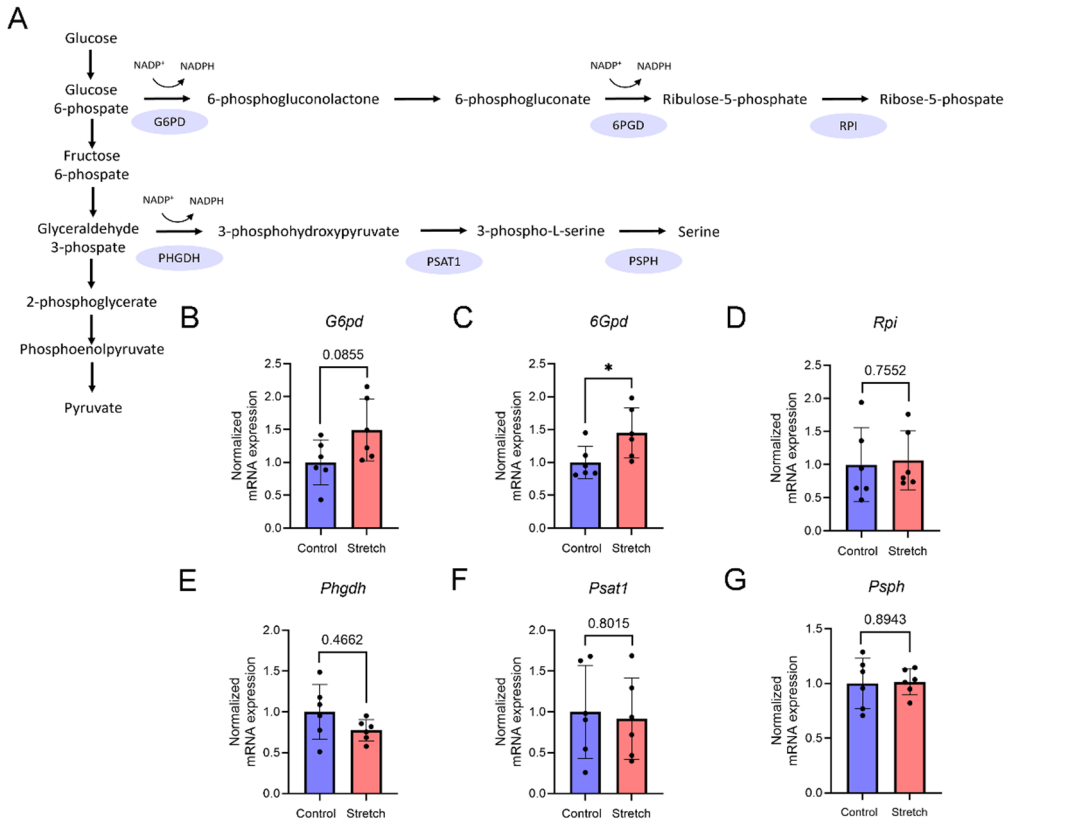

Fig. 4. Carbon shunting into the pentose phosphate pathway occurs in stretched ONH astrocytes. **(A)** Schematic of the derivative pathways of glucose metabolism including the PPP and the serine synthesis pathway (SSP). **(B-D)** PPP enzymes including glucose-6-phosphate dehydrogenase (*G6pd*), 6-phosphogluconate dehydrogenase (*6Gpd*), and ribose-5-phosphate isomerase (*Rpi*) were analyzed by qPCR, with *6Gpd* showing significantly increased mRNA expression in stretched ONH astrocytes ($p < 0.05$). **(E-G)** SSP enzymes including key enzymes such as phosphoglycerate dehydrogenase (*Phgdh*), phosphoserine aminotransferase (*Psat1*), and phosphoserine phosphatase (*Psph*) were unchanged in stretched ONH astrocytes compared to control. Data are two technical replicates for each of three independent biological replicates and are presented as mean ± SD, and a two-way AVOVA with mixed-effects model was used for analysis; $^{*}p < 0.05$.

findings of no significant differences in global metabolites (Supplementary Figure S3) suggest glucose-derived α-KG accumulation may assist in maintaining levels of some TCA metabolites including succinate, fumarate and malate.

α-Ketoglutarate accumulation influenced TCA cycle activity and histone modification but not antioxidant effects

Based on the observed increase in α-KG originating from glucose under stretch stress, we sought to confirm α-KG pooling by investigating and eliminating known ways by which α-KG would be used in a cell (Fig. 8E). α-KG can be converted to glutamate, one of the three amino acids that make up glutathione; as such, α-KG can increase GPx activity (Fig. 8A); α-KG can be reductively carboxylated to isocitrate, using NADPH as a reducing agent; and α-KG can be a co-factor in histone demethylation. RT-PCR analysis of *GPx* showed there was no significant difference between control and stretched ONH astrocyte transcripts (Fig. 8B), suggesting α-KG was not being used either for glutathione production (Fig. 8C) or increased *Gpx* activity. NADPH was not different between control and stretched ONH astrocytes (Fig. 8D), suggesting it was not being used as a reducing agent to a greater degree with stretching. ATP-citrate-lyase cleaves citrate into Acetyl-CoA and oxaloacetate, with Acetyl-CoA providing the acetyl group for acetylation. H3K27 acetylation did not differ between stretch and control ONH astrocytes (Fig. 8F). To examine whether accumulation of α-KG, a co-factor for histone demethylases such as the Jumonji C- terminal domain (JmjC) family[48,49], impacted histone methylation including histone H3K9, we performed immunohistochemistry using antibodies against histone H3 and H3K9 methylation. Co-localization of H3K9 on histone H3 was quantified (mean intensity of positive cells). The H3K9 methylation was decreased in stretched ONH astrocytes (Fig. 8G and H). Together, these data indicate accumulation of glucose-derived α-KG under stretch stress underlies its decreased utilization in histone methylation compared to control, demonstrating increased demethylation in stretched ONH astrocytes (Fig. 8H).

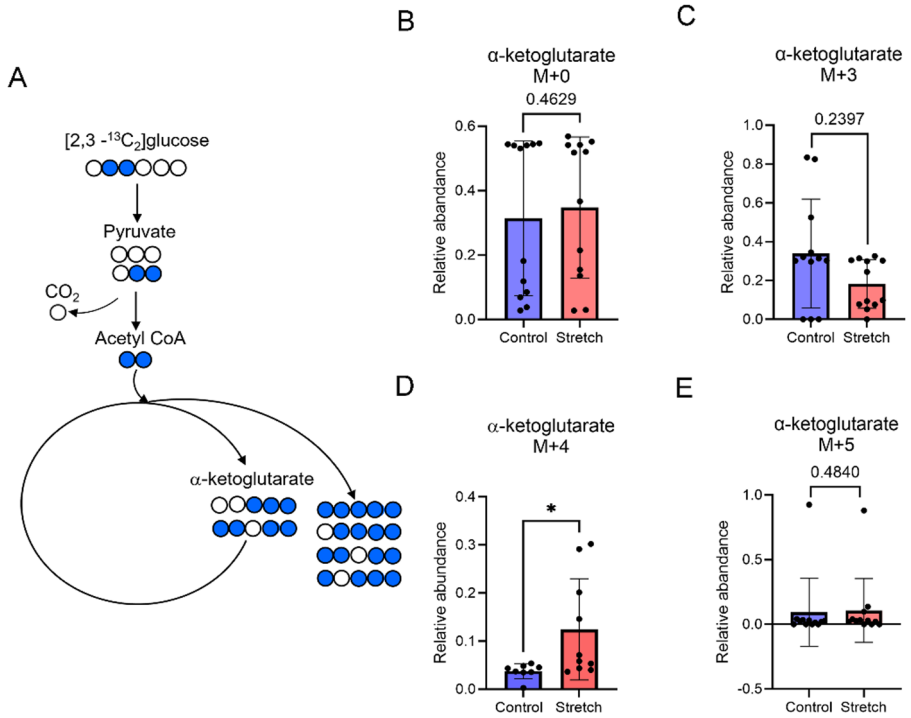

Fig. 5. Mass isotopologue distribution (MID) analysis of the [2,3-$^{13}C_2$]glucose fate involved in the PPP pathway **(A)** is shown. **(B-C** and **E)** GC-MS was utilized for analyzing the MID of α-KG in ONH astrocytes cultured on laminin MID analysis showed no difference of α-KG (M + 0), (M + 3) and (M + 5) between control and stretch conditions while α-KG (M + 4) was significantly increased in stretched astrocytes **(D)**. Data are two technical replicates for each of three independent biological replicates and are presented as mean ± SD; a two-way AVOVA with mixed-effects model was used for analysis. $^{*}p < 0.05$.

Discussion

In this study, we observed that the substrate upon which ONH astrocytes were cultured dictated YAP translocation, with the most significant pathway activation in cells cultured on laminin. The importance of laminin to integrin signaling, and that signal integration through YAP within the Hippo pathway, focused our attention on laminin for the remainder of the experiments. Strain on ONH astrocytes from the 12% stretch altered their metabolism, with overall reductions in metabolites associated with glycolysis and the TCA cycle. Using ^{13}C isotope tracing, we determined that strain on ONH astrocytes led to a pooling of α-KG as well as increased flux through the PPP, confirmed through mRNA and protein analysis.

Elevated IOP in glaucoma causes mechanical strain, resulting in ECM remodeling in the optic nerve head, and increased risk of LC deformation related to fibrosis[30]. ECM components such as collagen I-VI, elastin, heparan sulfate proteoglycans, fibronectin, and laminin are found in the ONH[50]. Collagen IV and V, heparan sulfate proteoglycans, and laminin are mainly located in basement membranes or basal lamina, which is dense with vascular endothelial cells and glial cells lining axon bundles in the optic nerve head[50,51]. ECM remodeling from increased levels of fibronectin and laminin have been observed in glaucomatous retina and optic nerve, leading to development of neurodegeneration[21]. Increased collagen VI and laminin levels and loss of elastin were observed in the LC of glaucomatous human ONH[22]. Perhaps unsurprisingly due to their increases observed in glaucoma, laminin and pronectin were the ECM substrates most capable of promoting YAP nuclear translocation as a result of stretch strain in our study. We ultimately focused on laminin for the metabolomics analysis so we could undertake a comprehensive metabolic analysis.

The Hippo signaling pathway, of which YAP and TAZ are important effectors, regulates cell growth and development. ECM remodeling activates cellular sensors like focal adhesions or integrins, thus affecting YAP through the actin cytoskeleton[52]. Changes in the mechanical microenvironments including ECM stiffening and stretching can bypass the rest of the Hippo pathway and directly promote YAP and TAZ nuclear translocation, activating gene transcription[38,53]. YAP and TAZ have been associated with glaucoma through work showing that LC cells isolated from glaucomatous human eyes and cultured on stiff (100 kPa) collagen substrate increased YAP gene expression and total YAP protein[40]. YAP/TAZ promote fibrosis through their regulation of ECM proteins, but they are also associated with metabolic regulation through their promotion of genes that impact glycolysis, lipogenesis and glutaminolysis[34]. Significant increases in ECM protein production would be energetically expensive, as supported by YAP induction of glutaminolysis and glycolysis in myofibroblasts[32]. We demonstrated that increased nuclear YAP translocation is observed in stretched ONH astrocytes cultured on laminin and pronectin. Additionally, GLUT1 expression was increased in astrocytes cultured on laminin, confirming our expectation that YAP activation would modulate metabolism in this context, including promoting glycolysis

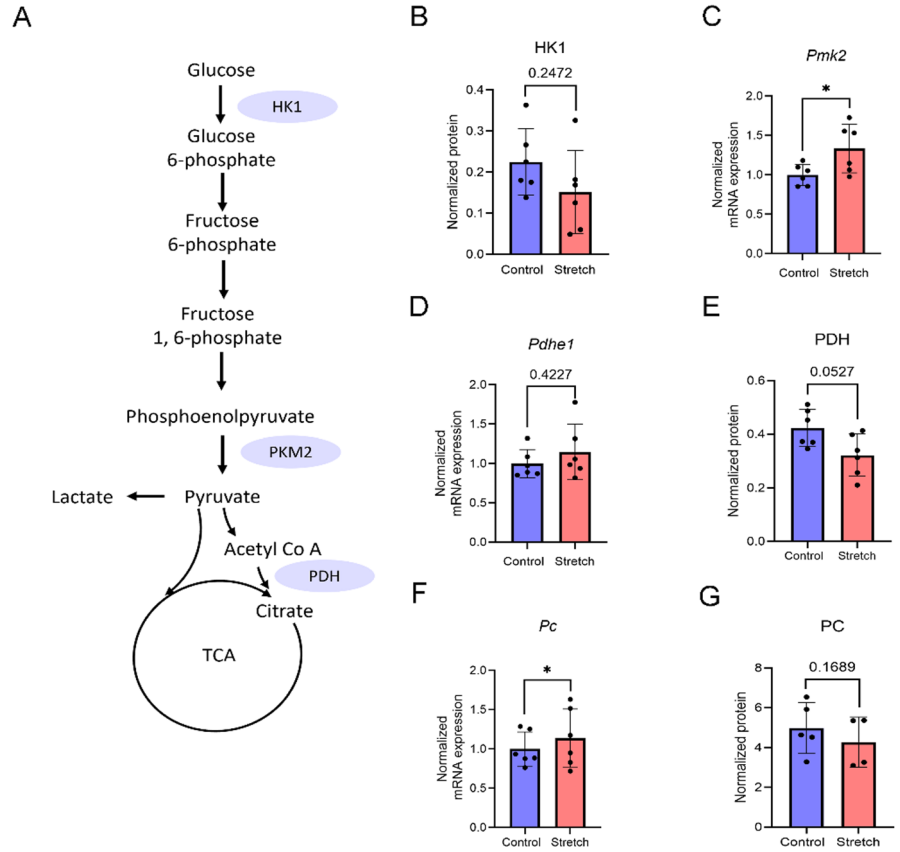

Fig. 6. Analysis of glycolytic enzyme mRNA and protein. **(A)** Schematic of the glycolysis pathway with the enzymes analyzed highlighted. **(B)** HK1 protein was unchanged in stretched ONH astrocytes compared to control. **(C)** Pyruvate kinase M2 (*Pkm2*) mRNA was significantly increased in stretched ONH astrocytes ($p < 0.05$). **(D)** Pyruvate dehydrogenase E1 (*Pdhe1*) mRNA and **(E)** pyruvate dehydrogenase protein were unchanged in stretched ONH astrocytes as compared to control. (**F** and **G**) Pyruvate carboxylase (*Pc*) mRNA was significant increased ($^*p < 0.05$) while PC protein remained unchanged in stretched ONH astrocytes. Data are two technical replicates for each of three independent biological replicates and are presented as mean ± SD; a two-way AVOVA with mixed-effects model was used for analysis. $^*p < 0.05$.

through increased lactate dehydrogenase, GLUT1 and HK-2 expression[54]. Moreover, integrin β4 expression was increased in ONH astrocytes cultured on laminin. Integrin β4 is associated with binding of astrocytes to basement membrane via laminin. Several integrins including α2β1, α3β1, α6β1, and α6β4, expressed in astrocytes, enable them to detect alterations in strain both within and anterior to the LC[55]. Interestingly, integrin β4 expression on astrocytes has been associated with upregulation of proinflammatory cytokines including interleukin-6 (IL-6) and interferon-α[56]. IL-6 is significantly upregulated in the context of glaucoma[57] and could be a driver of integrin β4 upregulation in vivo. Increased integrin β4 has been associated with YAP activation[46], and laminin-bound α6β4 integrin could activate YAP signaling in both cancer and non-cancerous cells such as epidermal stem cells[58,59]. Our findings suggest that mechanical strain-activated YAP translocation promoted enhanced GLUT1 expression in ONH astrocytes, possibly due to enhanced focal adhesion including integrin β4 expression on laminin.

To further explore the potential for the fibrotic changes in ONH astrocytes to shift metabolism concomitant with YAP translocation, we examined metabolites by GC-MS, including using stable isotope tracing via ^{13}C-labeled glucose. We observed a metabolic shift in ONH astrocytes exposed to mechanical stretch, leading to the overall reduction of metabolites including pyruvate, lactate, and citrate, suggesting glycolytic suppression. These findings are consistent with the growing understanding of metabolism in the glaucomatous retina and optic nerve. ONH astrocytes significantly alter their morphology and orientation in the course of glaucoma[60,61], which impacts their role as fortified cells that protect and support optic nerve axons[62]. Loss of the organizational structure by astrocytes within the ONH was proposed to severely impact metabolic support of axons[62]. Altered metabolism in retina and optic nerve has been observed in glaucomatous mice, resulting in neurodegeneration[63]. Increased IOP can result in decreased pyruvate levels and elevated glucose concentrations in the retina due to reduction of glycolytic metabolism[12]. Interventions that address reduced glycolysis like treatment with pyruvate in the *Lmx1b*^{V265D} mouse[64] or a combination of pyruvate and nicotinamide in the DBA/2J glaucoma mouse model, were able to decrease RGC loss and optic nerve degeneration[12]. In an analysis of glaucoma subjects from the UK BioBank, elevated levels of lactate, pyruvate and citrate in plasma were associated with lower glaucoma

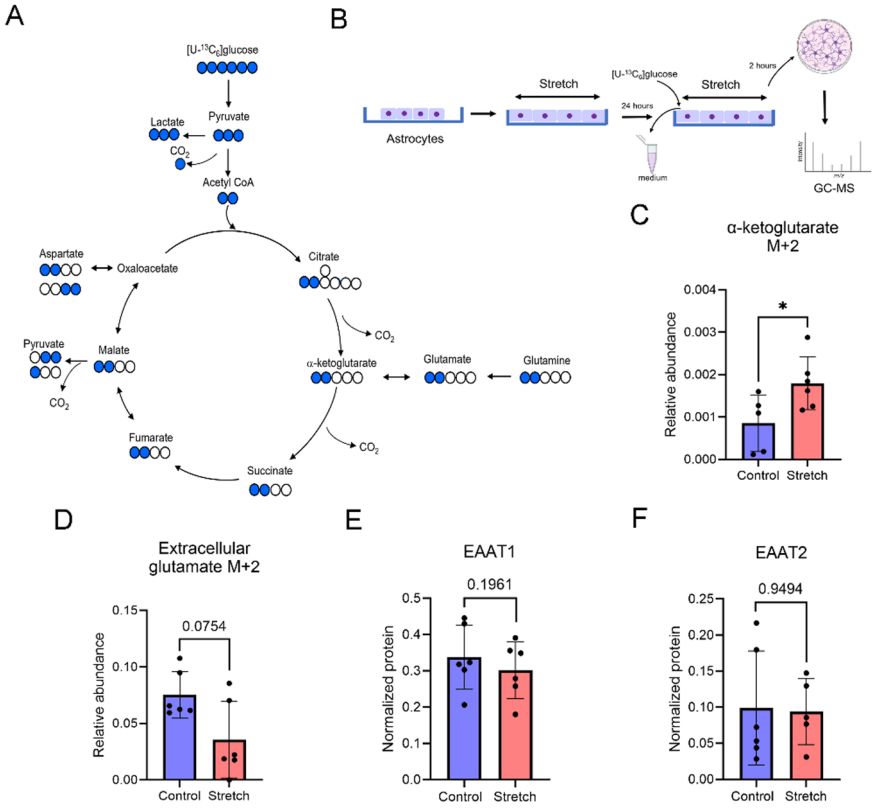

Fig. 7. Fate of glucose metabolism in stretched ONH astrocytes. **(A)** Schematic showing the expected flow of ^{13}C labeled carbon for one round of the TCA cycle. Comparison of relative enrichment of glucose and TCA metabolites was determined by M + 2 labeling from [U-$^{13}C_6$]glucose. **(B)** Schematic showing the experimental set-up wherein stretched astrocytes were provided with [U-$^{13}C_6$]glucose for 2 h after 24 h of stretch in order to undertake stable isotope tracing. **(C)** Relative enrichment of intracellular α-KG showed a significant increase of this metabolite in stretched ONH astrocytes ($p < 0.05$). **(D)** Extracellular glutamate was unchanged in ONH astrocytes exposed to mechanical stretch on laminin compared to control. (E and F) There were no changes in the protein levels of high affinity excitatory amino acid transporters 1 and 2 (EAAT 1 and EAAT 2) in control versus stretched ONH astrocytes. Data are two technical replicates for each of three independent biological replicates and are presented as mean ± SD; a two-way AVOVA with mixed-effects model was used for analysis. $^{*}p < 0.05$.

prevalence, suggesting that these metabolites formed a resilience signature against glaucoma development[64]. Relatedly, patients with normal tension glaucoma were observed to have significantly lower plasma lactate and total amino acid levels than control patients while blood glucose was unchanged[65]. Clinical trials of pyruvate and nicotinamide therapy showed these supplements can enhance RGC function in human glaucoma[66].

Astrocytes are the primary source of lactate production in the CNS, and released lactate becomes a vital source of energy for neurons[67]. Astrocytic glycolysis, triggered by neuronal excitation in stroke and in the course of neurodegeneration, can promote elevated lactate release[68]. Our study revealed that mechanical strain decreased lactate release along with the overall decline in pyruvate levels without changes in MCT4. However, transcripts for *Pkm2*, the enzyme that converts phosphoenolpyruvate to pyruvate, was increased while PDH expression was significantly decreased in stretched ONH astrocytes. PKM2, found specifically in astrocytes, can enhance glycolysis and drive metabolic reprogramming[69]. In a study of hypoxia in hepatocellular carcinoma, nuclear YAP binding to hypoxia-inducible factor-1α (HIF-1α) activated *Pkm2* RNA expression to accelerate glycolysis[70]. Chronic IOP elevation has been shown to increase HIF-1α as observed in the glaucomatous human ONH[71] and specifically in glia[72] in a mouse model of glaucoma. These findings raise the possibility that activation of YAP transactivated HIF-1α to promote increased *Pkm2* expression; however, higher *Pkm2* did not result in higher pyruvate levels in our ONH astrocytes as might be expected. We also observed decreased PDH expression; PDH inhibition often results in increased lactate through limiting pyruvate entry into the TCA cycle[73]. However, our findings also do not align with the increased lactate anticipated with low PDH. One possibility is the movement of pyruvate into another metabolic pathway, possibly conversion to oxaloacetate by pyruvate carboxylase. We show increased levels of pyruvate carboxylase transcripts, but stable levels of protein, in control and stretched ONH astrocytes; however, stable protein does not rule out increased enzyme activity in the stretched astrocytes. Conversion of pyruvate to oxaloacetate is an important means by which to replenish TCA cycle intermediates. Alternatively, pyruvate can be converted via alanine transaminase to alanine, thus contributing to protein synthesis. Pyruvate can also be converted to malate using NADPH to serve in the malate-aspartate shuttle.

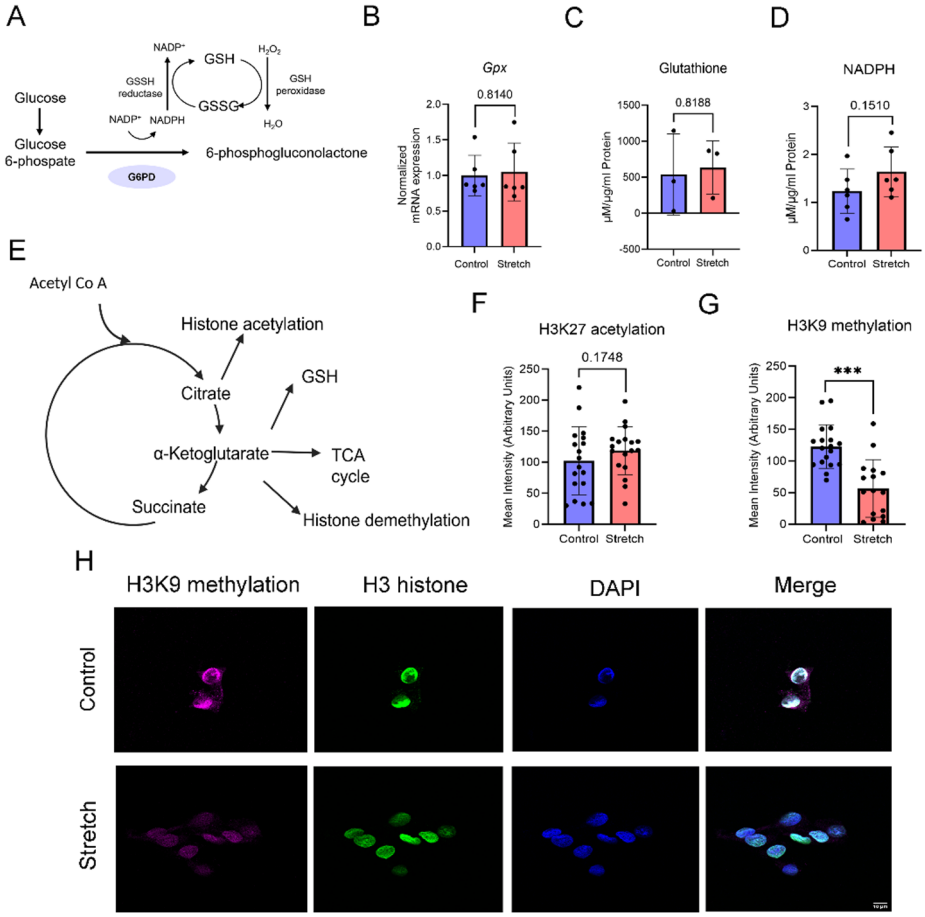

Fig. 8. Impact of TCA cycle intermediate alteration on cellular metabolism. **(A)** A schematic of NADPH production through the pentose phosphate pathway that enables glutathione production and glutathione peroxidase activity. **(B-D)** α-KG is a precursor of glutamate, one of the three amino acids that make up glutathione. The levels of *Gpx* mRNA, glutathione and NADPH were unchanged in stretched ONH astrocytes compared to control. **(E)** A Schematic of potential uses for α-ketoglutarate, including antioxidant production, TCA cycle activity, and histone demethylation. **(F)** The acetylation of histone H3K27 did not differ between stretched ONH astrocytes and control as measured by immunolabeling intensity. **(G)** The methylation of histone H3K9 was decreased in stretched ONH astrocytes compared to control, suggesting increased demethylation with stretch strain ($p < 0.05$). **(H)** Immunofluorescence of H3K9 methylation (magenta), H3 histone (green), and DAPI (blue) are shown individually and (far right) merged. H3K9 methylation in the stretched astrocytes is reduced compared to control. Scale bar = 10 µm, 63× magnification. Data are multiple fields of view taken from three independent biological replicates and are presented as mean ± SD. A two-way AVOVA with mixed-effects model was used for analysis. $^{*}p < 0.05$.

With all of these possible destinations, increased *Pkm2* in stretched cells likely increased pyruvate levels, and that pyruvate was quickly utilized in these other pathways. Low PDH expression is perhaps less of a surprise if pyruvate levels were low from its movement into these other pathways since lactate production would be limited when pyruvate is not available. We also showed that protein for HK-1, the first rate-limiting step of glycolysis, remained unchanged across groups. Altogether, our findings suggest that the stretched ONH astrocytes shunt glucose toward other metabolic pathways, leading to glycolysis suppression.

Our data indicates shunting of glucose-6-phosphate into the PPP in stretched ONH astrocytes. Glucose 6-phosphate is converted into ribulose 5-phosphate and NADPH via the PPP. The oxidative PPP associated with NADPH production is responsible for maintaining redox balance under stress[74]. The PPP has a non-oxidative branch which generates ribose 5-phosphate needed for purine synthesis[74]. The PPP, which draws glucose-6-phosphate out of the glycolysis pathway, is more active in astrocytes than in neurons, though the astrocytic PPP helps to protect neurons against oxidative stress by supplying reduced glutathione[68]. Gene expression of *6Gpd*, an enzyme involved in the oxidative branch associated with NADPH production was upregulated with stretch in ONH astrocytes. The NADPH generated from G6PD activity is used for glutathione production, which was unchanged with stretching in our ONH astrocytes, as was glutathione peroxidase. The *6Gpd* transcript was upregulated, which may or may not translate to increased protein; nor does it provide insight into any possible changes in enzyme activity. We did observe, however, that stretching enhanced the PPP activity as measured by the [2,3 $^{13}C_2$]glucose used to trace the fate of labeled carbon. We observed increased α-KG M + 4 levels in

stretch compared to control ONH astrocytes, indicating enhanced PPP activity. Our findings are reminiscent of a previous study of pancreatic adenocarcinoma under acidosis that showed increased cellular glucose and decreased glycolysis associated with YAP/TAZ pathway activation and extracellular matrix alteration, leading to a metabolic shift toward the PPP[75]. Our results revealed that stretch stress suppressed glycolysis and activated nuclear YAP, promoting redirected glucose to the PPP.

Previous findings from our laboratory found that stretched ONH astrocytes showed altered glycolytic and respiratory activity compared to control. However, both control and stretch ONH astrocytes still required glutamine, indicating a shared dependence on this nutrient[18]. Our evidence suggested declines in global glutamine, yet glutamate and α-KG levels were unchanged. It is possible that glutamine is being used to replenish TCA cycle intermediates. α-KG is a hub intermediate in the TCA cycle, and we observed reductions of citrate and glutamine, but not α-KG. Using carbon tracing, α-KG that originated from labeled glucose was increased by stretch, suggesting an accumulation of this intermediate, potentially for supporting the TCA cycle. An accumulation of α-KG is linked to ECM stiffness from stretching. α-KG is a rate-limiting cofactor for prolyl-4-hydroxylase that modifies proline residues to promote collagen production[76]. It has been reported that α-KG can modulate lysine demethylase activity and chromatin remodeling, especially H3K9 histone demethylation, resulting in myofibroblast formation[77]. Additional α-KG could enhance α-KG-dependent lysine demethylases to promote histone demethylation and opening chromatin to be transcriptionally permissive. However, the functional outcome of α-KG levels depend on their balance with competing metabolites such as succinate and fumarate (which inhibit α-KG-dependent lysine demethylases)[78] and whether the cellular compartment has α-KG dehydrogenase to convert α-KG to succinyl-CoA[79]. Additionally, increased α-KG promotes chromatin demethylation, leading to increased fibrotic gene expression and consequently, increasing collagen biosynthesis[77,80]. However, the pooling of α-KG as we observe, suggests, in the time frame in which we analyzed, α-KG may have not been utilized by stretched ONH astrocytes for these purposes. Our data examining the possible use of α-KG in glutathione production or demethylation bear this out. We show no changes in NADPH, Gpx1, or glutathione levels in ONH astrocytes with stretch. One possibility is that the enzyme that converts α-KG to succinyl-CoA, α-ketoglutarate dehydrogenase (α-KGDH), is inactivated in stretched ONH astrocytes. α-KGDH can be redox regulated, capable of being inactivated via post-translational modification of cysteine residues on the E2 subunit of α-KGDH[81]. If this could be demonstrated, then the increased α-KG may represent a temporary response to ROS generated with stretching. There is strong evidence for oxidative stress in the ONH[72,82] during models of glaucoma, suggesting the conditions for redox inactivation of TCA cycle enzymes exist.

In summary, we showed that stretch stress resulted in increased GLUT1 expression in ONH astrocytes cultured on laminin and enhanced upper glycolysis and shunting into the PPP, leading to reduced pyruvate flux into the TCA cycle. However, metabolic reprogramming in stretched ONH astrocytes indicated increased TCA intermediates, attributable to glucose-derived α-KG and imported glutamine. YAP translocation accompanied the increased GLUT1 expression. Limitations of this study include our correlation of YAP translocation with subsequent metabolic changes without direct inhibition/block of YAP translocation to alter the observed metabolic shifts. Relatedly, we were not able to measure whether different substrates appreciably altered the stiffness of the culture surface, so the YAP response to laminin versus a response to the potential difference in the surface stiffness cannot be distinguished. The metabolite analysis through stable isotope tracing yielded small yet statistically significant effects which underscore the nature of these findings as a snapshot of the metabolic activity. Future experiments will include more thorough connection between the YAP/TAZ pathway and metabolic regulation in ONH astrocytes, as well as an assessment of ONH astrocyte ECM secretion.

Methods

Primary optic nerve head astrocyte isolation and cell culture

ONH astrocytes were isolated from rats at 1–5 days old. ONHs were collected after decapitation of rat pups using scissors. All isolated cells were cultured in Dulbecco's modified eagle medium (DMEM) with 4.5% glucose, 2 mM glutamine and supplemented with 10% Fetal bovine serum (FBS) and 1x penicillin/streptomycin at 37 °C in a humid atmosphere containing 5% CO_2. To obtain the astrocytes, the cells migrated from explants were filtered through a sterile filter before centrifuging and cultured in a T75 flask. After the cells reached 80–90% confluency, the cells were shaken at 200 rpm to remove the non-astrocytes and then cultured in DMEM with 4.5% glucose, 2 mM glutamine and supplemented with 10% FBS and 1x penicillin/streptomycin. Approximately $0.4–1.2 \times 10^5$ astrocytes were seeded on 6-well FlexCell plates with various substrates including collagen (Cat no. BF-3001 C), elastin (Cat no. BF-3001E), laminin (Cat no. BF-3001 L) and pronectin (Cat no. BF-3001P). Pronectin is an artificial protein of 980 amino acids containing a repeated peptide segment from fibronectin[83]. Once astrocytes reached 80–90% confluency, approximately 3×10^5 cells, the cells were mechanically stretched by using a FX-6000T™ Tension System. FlexCell culture plates have a stiffness of 930kPa (www.flexcellint.com) which is greater stiffness than physiological ONH, though significantly lower than cell culture plastic (1GPa). Normal ONH is estimated to be ~ 100–300 kPa under normal intraocular pressure, with the ECM remodeling that occurs in the glaucomatous ONH estimated to increase stiffness by 20–30%[84,85].

Stretch Injury

To mimic the stretch strain encountered by ONH cells during glaucoma, the plated astrocytes were placed into a FlexCell 6000 T generating a 12% sinusoidal stretch with 1 Hz frequency for 24 h, following parameters previously employed in our lab[18]. A tensile strain at 12% is sufficient to mimic the pathophysiological effects in the glaucomatous ONH in vitro, although similar studies utilizing this method may range up to 17% strain[86,87]. Investigations of principal strain in the mouse ONH astrocytic lamina under controlled inflation from 10-30mmHg yielded a principal strain of 7.7% for older mice and 11.6% for younger mice[88], which correponds

to the calculated 50th percentile strain in the rat ONH biomechanic simulations[89], supporting our use of 12% strain for our rat ONH astrocytes. IOP naturally fluctuates, and the ocular pulse at the human ONH is 1 Hz, thus at this cyclic frequency the tissue feels the peak effect of pressure[90,91]. All media was collected. For isotope tracing analysis, the astrocytes underwent 24 h of stretch prior to being treated with 10mM [U-$^{13}C_6$]glucose (Cambridge Isotope Laboratories, Inc., CLM-1396) or [2, 3-$^{13}C_2$]glucose (Omicron Biochemicals, Inc., GLC-078) with stretching for an additional 2 h prior to cell and media collected. The cells were washed by PBS and harvested by trypsinization and cell count was measured by the trypan blue exclusion method. The cells were centrifugated at 200x g for 5 min to remove supernatant and the pellets were washed 2x with cold saline solution[92]. The cell pellets were kept at − 80 °C prior to GC-MS analysis.

Nuclear extraction

The nuclei were isolated by Nuclei Isolation Kit: Nuclei EZ Prep (Sigma Aldrich, NUC101-1KT) according to this brief protocol. The astrocytes were washed by cold PBS and scraped with ice-cold Nuclei EZ lysis buffer. The lysate was kept on ice for 5 min and centrifuged at 500 × g for 5 min at 4 °C to pellet nuclei. The pellets were added to ice-cold Nuclei EZ lysis buffer and incubated on ice for 5 min prior to centrifuging to obtain nuclei pellet. The nuclei were kept in ice-cold storage buffer and stored in − 70 °C until use.

Immunofluorescence labeling

Fluorescent immunolabeling was completed according to the following procedure[18]. The silicone membrane of the FlexCell culture plate containing astrocytes was cut at the center of the well, an area approximately 1 cm^2. In figures showing quantification of fluorescence intensity, four fields (200 × 280μm^2) within the 1cm^2 area were evaluated, or a total of 0.224% of the total area per well. Three wells per plate were evaluated for immunolabeling, including the histone modifications. Prior to nuclear staining for histone evaluation, the nuclear pellets were smeared onto glass slides. The astrocytes or nuclei were fixed with warm DMEM containing 3% paraformaldehyde for 15 min at 37 °C then rinsed twice with pre-warmed PBS. Aldehydes were quenched by incubating for 30 min in 50 mM ammonium chloride at room temperature (RT) followed by permeabilization for 10 min using PBS with 0.1% Triton X-100. The astrocytes were rinsed twice with PBS and blocked in 5% BSA and 5% DKS in PBS for 2 h at RT, then incubated with primary antibody overnight at RT. The astrocytes were immunolabeled with primary antibodies (Table 1) including glial fibrillary acidic protein (GFAP), GLUT1, and YAP protein. Nuclear immunolabeling proceeded with antibodies (Table 1) such as histone H3, histone H3K9 methylation (Histone H3 (tri methyl K9) and histone H3K27 acetylation (Acetyl-Histone H3 (Lys27)). Samples were incubated with primary antibodies overnight at 4 °C. Cells or nuclei were rinsed with blocking solution and incubated with secondary antibodies (Table 1) for 1 h at RT. Cells were rinsed with PBS three times prior to coverslipping with DAPI-Fluoromount-G (Southern Biotech). Samples were imaged using fluorescent microscopy at 40x with the appropriate excitation/emission filters, digitally recorded. The presence of nuclear YAP expression was scored by a blinded evaluator. The GLUT1 immunolabel was analyzed in at least 4 cells per image. In images of histone H3K9 methylation and histone H3K27 acetylation 20 nuclei were quantified per condition. The expression of GLUT1, histone H3, histone H3K9 methylation and histone H3K27 acetylation were quantified using Image J software[93]. Images had channels split to isolate the color channel and grayscale image. The selected cells were traced using selection tools such as freehand. The mean gray value was selected from set measurements to obtain the mean intensity.

RT-PCR

Control and stretched cells had media removed and replaced with lysis (RLT) buffer from the RNeasy Mini kit (Qiagen, Germantown, MD); cells were scraped from the membranes and RNA was isolated following the manufacturer's protocol. Isolated mRNA was measured using a NanoDrop (Fisher Scientific) and then cDNA was generated using the Verso cDNA Synthesis Kit (ThermoFisher Scientific). The cDNA was amplified using the appropriate forward and reverse primers (Table 2) via RT-qPCR using the QuantStudio™ 5 Real-Time PCR system (Thermo Fisher Scientific). *Rpl13* (ribosomal protein L13) was the housekeeping gene and a control sample served as the endogenous control. Primer specificity was confirmed through melt curves that indicated

Primary antibodies	Manufacturer	Cat No.
Chicken anti GFAP	Abcam	ab4674
Rabbit anti YAP	Cell Signaling	14,074-S
Rabbit anti GLUT1	Novus	NB110-39113
Mouse anti Histone H3	Active Motif	61,476
Rabbit Anti-Histone H3 (tri methyl K9)	Abcam	Ab8898
Rabbit anti Acetyl-Histone H3 (Lys27)	Cell signaling	8173
Secondary antibodies	**Manufacturer**	**Cat No.**
Donkey anti-Rabbit AlexaFlour 488	Jackson	711-545-152
Donkey anti-Mouse AlexaFlour 488	Jackson	715-545-150
Donkey anti-Chicken AlexaFlour 594	Jackson	703-585-155
Donkey anti-Rabbit AlexaFlour 594	Jackson	711-585-152

Table 1. Primary and secondary antibodies used.

Name	Primer sequence
6pgd	FP: 5': ggcccacacctatgaactct
6-phosphogluconate dehydrogenase	RP: 5': gtgacttcttcggcgatcac
G6pd	FP: 5': accaggcattcaaaacgcat
glucose 6-phosphate dehydrogenase	RP: 5': cagtctcagggaagtgtggt
Gpx	FP: 5': gaccgaccccaagtacatca
Glutathione peroxidase	RP: 5': gcagggcttctatatcgggt
Ppdhe1	FP: 5': gccttgccaacctgagaaaa
pyruvate dehydrogenase E1 subunit alpha	RP: 5': cggtaagagagcctgcaaac
Phgdh	FP: 5': gcaaccgattctaaggcctg
phosphoglycerate dehydrogenase	RP: 5': gtcctggagttcggctatca
Pmk2	FP: 5': catgcgtgtagtgcctgtac
pyruvate kinase M2	RP: 5': ttcacccctggctcaagtag
Pc	FP: 5': taccccaagcctctcaacag
pyruvate carboxylase	RP: 5': tatgtgagaactgcctgcca
Psat1	FP: 5': tcagtgccgtccccttaaat
phosphoserine aminotransferase 1	RP: 5': gttgaggttccaggtgcttg
Psph phosphoserine phosphatase	FP: 5': agctccagaccccactacta RP: 5': ccagctcatcgattccctct
Rpi	FP: 5': cgcttcattgtgatcgctga
ribose 5-phosphate isomerase	RP: 5': ctgccttgttgacagccatt
Rpl13	FP: 5': ctgtgaaggatcaacatttctg
Ribosomal Protein L13	RP: 5': gaccaccatccgctttttctt
Itgß 4	FP: 5': gtcgacgcctggtaaacatc
Integrin subunit beta 4	RP: 5': ggtagaacaacagctcccct

Table 2. Primer sequences for amplified genes.

amplification of a single amplicon. *Slc16a3* (monocarboxylate transporter 4; MCT4) expression was quantified using TaqMan assay with TaqMan assay primer (Mm00446102_m1 Slc16a3) and *Hprt* (Mm00446968_m1 Hprt) was the control sample. Each reaction was performed in triplicate. Data were analyzed from two technical and three biological replicates. The gene expression data were processed using Applied Biosystems software and expressed as fold change in the final results[94].

Cell extraction for GC-MS

Metabolites from cell pellets were extracted and analyzed by GC-MS. Acetonitrile: Isopropanol: Water (3:2:2, v/v/v) was added to the pellet with D, L 1 µg Norleucine as an internal standard. Samples were centrifuged at 10,000xg at 4 °C for 25 min. The supernatant was transferred to a new tube and evaporated using a Speedvac (Eppendorf). Metabolites were reconstituted in Acetonitrile: Water (1:1, v/v) and dried again with a Speedvac. After evaporation, dried samples were dissolved in 50 µl methoxyamine hydrochloride (20 mg/ml) in pyridine and then incubated at 30 °C for 2 h followed by addition of 50 µl of N-(tert-butyldimethysilyl)-N-methyltrifluoroacetamide (MTBSTFA). Each sample was incubated at 60 °C for 1 h and centrifuged at 8000xg for 10 min. Thereafter, the supernatants were transferred into a GC-MS vial for metabolomic analysis[92].

GC-MS analysis of TCA cycle

Chromatographic analysis of all metabolites and subsequent quantification of their m0-mi isotopologues were obtained using GC-MS. The GC-MS was a Thermo Trace 1300/TSQ 8000Evo Triple Quadrupole Mass Spectrometer using Chromeleon 7.2.10 Chromatography Data System (CDS) suite (Thermo Fisher Scientific, Waltham, Massachusetts, USA) for data acquisition and processing. The oven program was 60 °C (1 min) to 300 °C (5 min) at a ramp rate of 10 °C/min. The column was a Shimadzu Rxi-5SilMS 30 m × 0.25 mm × 0.25 µm (model no: 221–75954-30), a traditional non-polar phase (5% diphenyl/95% dimethyl polysiloxane). Helium at 1 mL/min was used as the carrier gas. The inlet was at 240°C with a split ratio of 10:1. The transfer line for the mass spectrometer was at 250°C. The electron impact (EI) ion source (70 eV) was maintained at 200 °C, and the mass spectrometer was operated in SIM mode (see Supplementary Table S1). Mass spectra of amino acids were generated in the scan mode (range, m/z 50–600).

GC-MS analysis of pentose phosphate pathway

The GC-MS used was an Agilent Intuvo 9000 Gas Chromatograph System-5977 C single quadrupole (Agilent, Santa Clara, California, USA) with OpenLab CDS 2.8 suite for data acquisition and processing. The oven program was 60 °C (0.44 min) to 300 °C (2.18 min) at a ramp rate of 22.9 °C/min. The column was an Agilent J&W HPS-5ms Ultra Inert 20 m × 0.18 mm × 0.18 µm, compatible only with the Intuvo 9000 GC System (PN: 190–91 S-577UI-INT), using a traditional non-polar phase (5% diphenyl/95% dimethyl polysiloxane). Hydrogen at 0.8 mL/min was used as the carrier gas. The inlet was at 240°C with a split ratio of 10:1. The transfer line for

Antibodies	Manufacturer	Catalog No.	Dilution	Observed Peak (kDa)
Rabbit anti excitatory amino acid transporter (EAAT 1)	Bioss	Bs-1003R	1:25	85–86
Rabbit anti excitatory amino acid transporter (EAAT 2)	Proteintech	22515-1AP	1:25	66–71
Rabbit anti hexokinase 1 (HK1)	Cell signaling	8337	1:25	90–99
Rabbit anti pyruvate dehydrogenase (PDH)	Cell signaling	8674	1:25	34–46
Rabbit anti pyruvate carboxylase (PC)	Proteintech	16588-1AP	1:50	93–114

Table 3. Antibodies used for capillary electrophoresis.

the mass spectrometer was at 250°C and the ion source temperature was 230°C. The mass spectrometer used an EI hydroinert source (70 eV) and was autotuned using the etune tuning algorithm operating in SIM mode (see Supplementary Table S1) with a 20 ms dwell time.

The metabolomic profile was analyzed by MetaboAnalyst 6.0. Metabolite abundance was expressed relative to the internal standard and normalized to cell number and then subjected to Statistical Analysis using MetaboAnalyst 6.0; see Supplementary Fig. 2[95]. For analysis of isotope abundance, National Institute of Standards and Technology library mass spectra were used and unlabeled, derivatized metabolite standards. The Chromeleon 7.2.10 or OpenLab 2.8 CDS suites were used to integrate the peak areas of the m0 to mi isotopologues of the $[M-57]^+$ fragment for each metabolite of interest and the m0 peak area of the $[M-57]^+$ fragment[96]. The Mass Isotopologue Distribution (MID) originating for the ^{13}C-tracer was identified[97]. After that, a correction process was applied to account for naturally occurring isotopes in each metabolite. Isotope correction was calculated using the IsoCorrectoR computational method[98,99]. The same dataset of integrated peak areas (m0 – mi) was also utilized to compute the absolute concentrations of metabolites in the ^{13}C-isotopically labeled samples.

Lactate assay

To quantify the global lactate efflux from ONH astrocytes, we used the Lactate Assay Kit from Cayman Chemical (Cat No. 700510). Conditioned media collected from the control and stretched cells after incubating for 24 h was harvested and deproteinated using 3-Mercaptopropionic acid. The extracellular lactate was measured in a 96-well plate (Cytation 5.0 by BioTek) against a standard curve following the manufacturer's directions Following trypsinization, cell number was determined using the trypan blue exclusion method and counting via hemocytometer. Lactate was normalized by cell number and reported as nM lactate/number of cells.

Glutathione assay

Extracellular glutathione levels were measured using a Glutathione Assay Kit (Cayman Chemical, Cat No. 703002) according to the manufacturer's instructions. After incubating for 24 h, the media from the control and stretched plates was collected and deproteinated using 3-Mercaptopropionic acid. The extracellular glutathione concentration was measured in a 96-well plate (Cytation 5.0 by BioTek) and calculated from standard curve. Glutathione was normalized to protein concentration determined using the BCA method (Pierce) and presented as nM/ug/ml protein.

NADPH assay

The intracellular NADPH content was detected by using a NADP+/NADPH assay kit (WST-8) (MedChemExpress, Cat No. HY-K1501). Cell lysates were harvested by scraping into T-PER solution (ThermoFisher) from astrocytes exposed to stretching or the control group. The concentration of NADPH was quantified in a 96-well plate using the Cytation 5.0 (BioTek), following the manufacturer's instructions for the NADPH standard curve. The NADPH level was presented as a NADPH concentration per unit of protein as determined by BCA assay (Pierce).

Capillary electrophoresis for protein analysis

To quantify protein, we used the Jess instrument from Protein Simple (San Jose, CA, United States) which combines capillary electrophoresis with in-capillary immunodetection using chemiluminescence. Protein peaks yielded area-under-the-curve values (the dropped lines parameter was used); only peaks with a signal to noise ratio 10 were used. Proteins were normalized to total protein as detected by biotinylation of all proteins, binding by an HRP-streptavidin conjugate and then a luminol/peroxide reaction. The list of antibodies, their dilution, and corresponding observed peak are shown in Table 3.

Statistical analysis

Data is shown as mean ± SD. Data obtained from GC-MS were presented as mean ± SD from two technical replications of three biological replications. To conform with best practices regarding technical replicates, we used a two-way ANOVA with mixed-effects (hierarchical) model that explicitly accounts for within-sample correlation when comparing control and stretch group replicate values (technical and biological) across all quanititative data. A p value < 0.05 was considered significant.

Data availability

Data is available as presented in the published manuscript and in the Texas Data Respository, https://doi.org/10.18738/T8/6WVJZG

Received: 31 October 2025; Accepted: 20 April 2026

Published online: 28 April 2026

References

1. Pang, J.-J., Frankfort, B. J., Gross, R. L. & Wu, S. M. Elevated intraocular pressure decreases response sensitivity of inner retinal neurons in experimental glaucoma mice. *Proc. Natl. Acad. Sci. U. S. A.* **112**, 2593–2598 (2015).
2. Jassim, A. H. et al. Higher reliance on glycolysis limits glycolytic responsiveness in degenerating glaucomatous optic nerve. *Mol. Neurobiol.* **56**, 7097–7112 (2019).
3. Williams, P. A. et al. Vitamin B3 modulates mitochondrial vulnerability and prevents glaucoma in aged mice. *Science* **355**, 756–760 (2017).
4. García-Bermúdez, M. Y. et al. Glial cells in glaucoma: friends, foes, and potential therapeutic targets. *Front. Neurol.* **12**, 624983 (2021).
5. Anderson, D. R. Ultrastructure of human and monkey lamina cribrosa and optic nerve head. *Arch. Ophthalmol.* **82**, 800–814 (1969).
6. Tekkök, S. B., Brown, A. M., Westenbroek, R., Pellerin, L. & Ransom, B. R. Transfer of glycogen-derived lactate from astrocytes to axons via specific monocarboxylate transporters supports mouse optic nerve activity. *Journal of Neuroscience Research* **81**, 644–652 (2005).
7. Fünfschilling, U. et al. Glycolytic oligodendrocytes maintain myelin and long-term axonal integrity. *Nature*, **485** 517–521 (2012).
8. Saab, A. S., Tzvetanova, I. D. & Nave, K. A. The role of myelin and oligodendrocytes in axonal energy metabolism. *Curr. Opin. Neurobiol.* **23**, 1065–1072 (2013).
9. Carreras, F. J. et al. Expression of glucose transporters in the prelaminar region of the optic-nerve head of the pig as determined by immunolabeling and tissue culture. *PLoS One* **10**, e0128516 (2015).
10. Harun-or-Rashid, M. et al. Structural and functional rescue of chronic metabolically stressed optic nerves through respiration. *J. Neurosci.* **38**, 5122–5139 (2018).
11. Wareham, L. K. & Calkins, D. J. The neurovascular unit in glaucomatous neurodegeneration. *Front. Cell Dev. Biol.* **8**, 452 (2020).
12. Harder, J. M. et al. Disturbed glucose and pyruvate metabolism in glaucoma with neuroprotection by pyruvate or rapamycin. *Proc. Natl. Acad. Sci. U. S. A.* **117**, 33619–33627 (2020).
13. Tang, Y., Chen, Y. & Chen, D. The heterogeneity of astrocytes in glaucoma. *Front. Neuroanat.* **16**, 995369 (2022).
14. Burgoyne, C. F. A biomechanical paradigm for axonal insult within the optic nerve head in aging and glaucoma. *Exp. Eye Res.* **93**, 120–132 (2011).
15. Hernandez, M. R. & Pena, J. D. The optic nerve head in glaucomatous optic neuropathy. *Arch. Ophthalmol.* **115**, 389–395 (1997).
16. Ansaryan, S. et al. Stretch Induces Invasive Phenotypes in Breast Cells Due to Activation of Aerobic-Glycolysis-Related Pathways. *Adv. Biosyst.* **3**, e1800294 (2019).
17. Feng, Y. et al. Mechanical stretch activates glycometabolism-related enzymes via estrogen in C(2) C(12) myoblasts. *J. Cell. Physiol.* **235**, 5702–5710 (2020).
18. Pappenhagen, N., Yin, E., Morgan, A. B., Kiehlbauch, C. C. & Inman, D. M. Stretch stress propels glutamine dependency and glycolysis in optic nerve head astrocytes. *Front. Neurosci.* **16**, 957034 (2022).
19. Tharp, K. M. et al. Adhesion-mediated mechanosignaling forces mitohormesis. *Cell Metabol.* **33**, 1322–1341e1313 (2021).
20. Downs, J. C., Roberts, M. D. & Burgoyne, C. F. Mechanical Environment of the Optic Nerve Head in Glaucoma. *Optom. Vis. Sci.* **85**, E425–E435 (2008).
21. Reinhard, J., Wiemann, S., Hildebrandt, S. & Faissner, A. Extracellular Matrix Remodeling in the Retina and Optic Nerve of a Novel Glaucoma Mouse Model *Biology*.
22. Hernandez, M. R., Igoe, F. & Neufeld, A. H. Extracellular matrix of the human optic nerve head. *Am. J. Ophthalmol.* **102**, 139–148 (1986).
23. Rehnberg, M., Ammitzböll, T. & Tengroth, B. Collagen distribution in the lamina cribrosa and the trabecular meshwork of the human eye. *Br. J. Ophthalmol.* **71**, 886 (1987).
24. Hernandez, M. R., Pena, J. D., Selvidge, J. A., Salvador-Silva, M. & Yang, P. Hydrostatic pressure stimulates synthesis of elastin in cultured optic nerve head astrocytes. *Glia* **32**, 122–136 (2000).
25. Dillinger, A. E. et al. CCN2/CTGF-A Modulator of the Optic Nerve Head Astrocyte. *Front. Cell. Dev. Biol.* **10**, 864433 (2022).
26. McLoon, S. C., McLoon, L. K., Palm, S. L. & Furcht, L. T. Transient expression of laminin in the optic nerve of the developing rat. *J. Neurosci.* **8**, 1981 (1988).
27. Downs, J. C., Roberts, M. D. & Burgoyne, C. F. Mechanical environment of the optic nerve head in glaucoma. *Optom. Vis. Sci.* **85**(6):E425–E435, https://doi.org/10.1097/OPX.0b013e31817841cb (2008).
28. Zhavoronkov, A. et al. Pro-fibrotic pathway activation in trabecular meshwork and lamina cribrosa is the main driving force of glaucoma. *Cell. Cycle.* **15**, 1643–1652 (2016).
29. Qiu, C. et al. The dynamic scleral extracellular matrix alterations in chronic ocular hypertension model of rats. *Front. Physiol.* **11**, 682 (2020).
30. Pitha, I., Du, L., Nguyen, T. D. & Quigley, H. IOP and glaucoma damage: The essential role of optic nerve head and retinal mechanosensors. *Prog. Retin. Eye Res.* **99**, 101232 (2024).
31. Bertrand, A. A., Malapati, S. H., Yamaguchi, D. T. & Lee, J. C. The Intersection of Mechanotransduction and Regenerative Osteogenic Materials. *Adv. Healthc. Mater.* **9**, 2000709 (2020).
32. Ibar, C. & Irvine, K. D. Integration of Hippo-YAP signaling with metabolism. *Dev. Cell* **54**, 256–267 (2020).
33. Plouffe, S. W. et al. The Hippo pathway effector proteins YAP and TAZ have both distinct and overlapping functions in the cell. *J. Biol. Chem.* **293**, 11230–11240 (2018).
34. Koo, J. H. & Guan, K.-L. Interplay between YAP/TAZ and metabolism. *Cell Metab.* **28**, 196–206 (2018).
35. Zhang, W. & Kong, Y. YAP is essential for TGF-β-induced retinal fibrosis in diabetic rats via promoting the fibrogenic activity of Müller cells. *J. Cell. Mol. Med.* **24**, 12390–12400 (2020).
36. Meng, K. P., Majedi, F. S., Thauland, T. J. & Butte, M. J. Mechanosensing through YAP controls T cell activation and metabolism. *J. Exp. Med.* **217**, e20200053 (2020).
37. Low, B. C. et al. YAP/TAZ as mechanosensors and mechanotransducers in regulating organ size and tumor growth. *FEBS Lett.* **588**, 2663–2670 (2014).
38. Cai, X., Wang, K. C. & Meng, Z. Mechanoregulation of YAP and TAZ in Cellular Homeostasis and Disease Progression. *Front. Cell. Dev. Biology* , **9**, 673599 (2021).
39. Rausch, V. & Hansen, C. G. The Hippo Pathway, YAP/TAZ, and the plasma membrane. *Trends Cell Biol.* **30**, 32–48 (2020).
40. Murphy, R. et al. Matrix mechanotransduction via Yes-Associated Protein in human Lamina Cribrosa cells in glaucoma. *Invest. Ophthalmol. Vis. Sci.* **63**, 16–16 (2022).
41. Qian, H. et al. SRY-Box transcription factor 9 triggers YAP nuclear entry via direct interaction in tumors. *Signal Transduct. Target. Ther.* **9**, 96 (2024).
42. Somamoto, S. & Tabata, Y. Effect of ProNectin F derivatives on cell attachment and proliferation. *Acta Biomater.* **9**, 5194–5200 (2013).
43. Cox, A. G. et al. Yap regulates glucose utilization and sustains nucleotide synthesis to enable organ growth. *EMBO J.* **37**, e100294 (2018).

44. Aydın, R. et al. Early localized alterations of the retinal inner plexiform layer in association with visual field worsening in glaucoma patients. *PLoS One.* **16**, e0247401 (2021).
45. Morrison, J. C. and Integrins in the optic nerve head: potential roles in glaucomatous optic neuropathy 453–477 (2006).
46. Lee, J. Y. et al. Identification of cell context-dependent YAP-associated proteins reveals β1 and β4 integrin mediate YAP translocation independently of cell spreading. *Sci. Rep.* **9**, 17188 (2019).
47. Lee, M. H., Malloy, C. R., Corbin, I. R., Li, J. & Eunsook, J. S. Assessing the pentose phosphate pathway using [2, 3–13 C2]glucose. *NMR Biomed.* **32**, e4096 (2019).
48. Hou, H. & Yu, H. Structural insights into histone lysine demethylation. *Curr. Opin. Struct. Biol.* **20**, 739–748 (2010).
49. Tran, K. A., Dillingham, C. M. & Sridharan, R. The role of alpha-ketoglutarate-dependent proteins in pluripotency acquisition and maintenance. *J. Biol. Chem.* **294**, 5408–5419 (2019).
50. Morrison, J. C., Jerdan, J. A., L'Hernault, N. L. & Quigley, H. A. The extracellular matrix composition of the monkey optic nerve head. *Invest. Ophthalmol. Vis. Sci.* **29**, 1141–1150 (1988).
51. Hernandez, M. R., Andrzejewska, W. M. & Neufeld, A. H. Changes in the Extracellular Matrix of the Human Optic Nerve Head in Primary Open-Angle Glaucoma. *Am. J. Ophthalmol.* **109**, 180–188 (1990).
52. Nardone, G. et al. YAP regulates cell mechanics by controlling focal adhesion assembly. *Nat. Commun.* **8**, 15321 (2017).
53. Kwon, H., Kim, J. & Jho, E. Role of the Hippo pathway and mechanisms for controlling cellular localization of YAP/TAZ. *FEBS J.* **289**, 5798–5818 (2022).
54. Liu, Q. P., Luo, Q., Deng, B., Ju, Y. & Song, G. B. Stiffer matrix accelerates migration of hepatocellular carcinoma cells through enhanced aerobic glycolysis via the MAPK-YAP signaling. *Cancers (Basel),* **12,** (2020).
55. Morrison, J. C. Integrins in the optic nerve head: Potential roles in glaucomatous optic neuropathy (an American Ophthalmological Society thesis). *Trans. Am. Ophthalmol. Soc.* **104**, 453–477 (2006).
56. Milner, R. & Campbell, I. L. Increased expression of the β4 and α5 integrin subunits in cerebral blood vessels of transgenic mice chronically producing the pro-inflammatory cytokines IL-6 or IFN-α in the central nervous system. *Mol. Cell. Neurosci.* **33**, 429–440 (2006).
57. Johnson, E. C. et al. Cell proliferation and Interleukin-6–type cytokine signaling are implicated by gene expression responses in early optic nerve head injury in rat glaucoma. *Investig. Ophthalmol. Vis. Sci.* **52**, 504–518 (2011).
58. De Rosa, L. et al. Laminin 332-dependent YAP dysregulation depletes epidermal stem cells in junctional epidermolysis bullosa. *Cell Rep.* **27**, 2036-2049.e2036 (2019).
59. Zhao, X. et al. Laminin-bound integrin α6β4 promotes non-small cell lung cancer progression via the activation of YAP/TAZ signaling pathway. *Front. Oncol.* **12**, 1015709 (2022).
60. Sun, D., Lye-Barthel, M., Masland, R. H. & Jakobs, T. C. The morphology and spatial arrangement of astrocytes in the optic nerve head of the mouse. *J. Comp. Neurol.* **516**, 1–19 (2009).
61. Lye-Barthel, M., Sun, D. & Jakobs, T. C. Morphology of astrocytes in a glaucomatous optic nerve. *Investig. Ophthalmol. Vis. Sci.* **54**, 909–917 (2013).
62. Dai, C. et al. Structural basis of glaucoma: The fortified astrocytes of the optic nerve head are the target of raised intraocular pressure. *Glia* **60**, 13–28 (2012).
63. Rombaut, A., Brautaset, R., Williams, P. A. & Tribble, J. R. Glial metabolic alterations during glaucoma pathogenesis. *Front Ophthalmol (Lausanne)* **3**, 1290465 (2023).
64. Li, K. et al. *Pyruvate and Related Energetic Metabolites Modulate Resilience* (Against High Genetic Risk for Glaucoma eLife Sciences Publications, Ltd, 2025).
65. Vohra, R. et al. Potential metabolic markers in glaucoma and their regulation in response to hypoxia. *Acta Ophthalmol.* **97**, 567–576 (2019).
66. De Moraes, C. G. et al. Nicotinamide and pyruvate for neuroenhancement in open-angle glaucoma: A phase 2 randomized clinical trial. *JAMA Ophthalmol.* **140**, 11–18 (2022).
67. Horvat, A., Zorec, R. & Vardjan, N. Lactate as an astroglial signal augmenting aerobic glycolysis and lipid metabolism. *Front. Physiol.* **12**, 735532 (2021).
68. Takahashi, S. Neuroprotective function of high glycolytic activity in astrocytes: Common roles in stroke and neurodegenerative diseases. *Int. J. Mol. Sci.* **22**(12): 6568 https://doi.org/10.3390/ijms22126568 (2021).
69. Magistretti, P. J. & Allaman, I. A cellular perspective on brain energy metabolism and functional imaging. *Neuron* **86**, 883–901 (2015).
70. Zhang, X. et al. Yes-associated protein (YAP) binds to HIF-1α and sustains HIF-1α protein stability to promote hepatocellular carcinoma cell glycolysis under hypoxic stress. *J. Exp. Clin. Cancer Res.* **37**, 216 (2018).
71. Tezel, G. & Wax, M. B. Hypoxia-inducible factor 1alpha in the glaucomatous retina and optic nerve head. *Arch. Ophthalmol.* **122**, 1348–1356 (2004).
72. Jassim, A. H. & Inman, D. M. Evidence of hypoxic glial cells in a model of ocular hypertension. *Invest. Ophthalmol. Vis. Sci.* **60**, 1–15 (2019).
73. Liu, Z., Guo, Y., Zhang, Y., Gao, Y. & Ning, B. Metabolic reprogramming of astrocytes: Emerging roles of lactate. *Neural Regen. Res.* **21**, 421–432 (2026).
74. Stincone, A. et al. The return of metabolism: Biochemistry and physiology of the pentose phosphate pathway. *Biol. Rev. Camb. Philos. Soc.* **90**, 927–963 (2015).
75. Chen, S. et al. Enhanced pentose phosphate pathway activity promotes pancreatic ductal adenocarcinoma progression via activating YAP/MMP1 axis under chronic acidosis. *Int. J. Biol. Sci.* **18**, 2304–2316 (2022).
76. Son, E. D. et al. Alpha-ketoglutarate stimulates procollagen production in cultured human dermal fibroblasts, and decreases UVB-induced wrinkle formation following topical application on the dorsal skin of hairless mice. *Biol. Pharm. Bull.* **30**, 1395–1399 (2007).
77. Gibb, A. A. et al. Glutamine uptake and catabolism is required for myofibroblast formation and persistence. *J. Mol. Cell. Cardiol.* **172**, 78–89 (2022).
78. Xiao, M. et al. Inhibition of alpha-KG-dependent histone and DNA demethylases by fumarate and succinate that are accumulated in mutations of FH and SDH tumor suppressors. *Genes Dev.* **26**, 1326–1338 (2012).
79. Huang, F. et al. Control of histone demethylation by nuclear-localized alpha-ketoglutarate dehydrogenase. *Sci.* **381**, eadf8822 (2023).
80. Ligresti, G. et al. CBX5/G9a/H3K9me-mediated gene repression is essential to fibroblast activation during lung fibrosis *JCI Insight* **5**, (2019).
81. Majsterek, I. et al. Evaluation of oxidative stress markers in pathogenesis of primary open-angle glaucoma. *Exp. Mol. Pathol.* **90**, 231–237 (2011).
82. Chidlow, G., Wood, J. P. M. & Casson, R. J. Investigations into Hypoxia and Oxidative Stress at the Optic Nerve Head in a Rat Model of Glaucoma. *Front. Neurosci.* **11**, 478 (2017).
83. DeSimone, D. W., Stepp, M. A., Patel, R. S. & Hynes, R. O. The integrin family of cell surface receptors. *Biochem. Soc. Trans.* **15**, 789–791 (1987).
84. Edwards, M. E. & Good, T. A. Use of a mathematical model to estimate stress and strain during elevated pressure induced lamina cribrosa deformation. *Curr. Eye Res.* **23**, 215–225 (2001).

85. Sigal, I. A., Flanagan, J. G. & Ethier, C. R. Factors influencing optic nerve head biomechanics. *Invest. Ophthalmol. Vis. Sci.* **46**, 4189–4199 (2005).
86. Li, Z. et al. Mechanobiological responses of astrocytes in optic nerve head due to biaxial stretch. *BMC Ophthalmol.* **22**368. (2022).
87. Rogers, R. S., Dharsee, M., Ackloo, S., Sivak, J. M. & Flanagan, J. G. Proteomics analyses of human optic nerve head astrocytes following biomechanical. *Mol. Cell. Proteomics* **11**, M111.012302 (2012).
88. Nguyen, C. et al. Age-related changes in quantitative strain of mouse astrocytic lamina cribrosa and peripapillary sclera using confocal microscopy in an explant model. *Invest. Ophthalmol. Vis. Sci.* **59**, 5157–5166 (2018).
89. Schwaner, S. A. et al. Individual-specific modeling of rat optic nerve head biomechanics in glaucoma. *J. Biomech. Eng.*, **143**(14): 041004 https://doi.org/10.1115/1.4049157 (2021).
90. Madekurozwa, M., Stamer, W. D., Reina-Torres, E., Sherwood, J. M. & Overby, D. R. The ocular pulse decreases aqueous humor outflow resistance by stimulating nitric oxide production. *Am. J. Physiol. Cell. Physiol.* **320**, C652–C665 (2021).
91. Turner, D. C. et al. Transient intraocular pressure fluctuations: Source, magnitude, frequency, and associated mechanical energy. *Invest. Ophthalmol. Vis. Sci.* **60**, 2572–2582 (2019).
92. Chang, M. C. et al. Synergistic Effect of β-Lapachone and Aminooxyacetic Acid on Central Metabolism in Breast Cancer *Nutrients* **14**, (2022).
93. Schindelin, J. et al. Fiji: An open-source platform for biological-image analysis. *Nat. Methods* **9**, 676–682 (2012).
94. Muller, P. Y., Janovjak, H., Miserez, A. R. & Dobbie, Z. Processing of gene expression data generated by quantitative real-time RT-PCR *Biotechniques* **32**, 1372–1374, 1376, 1378–1379 (2002).
95. Pang, Z. et al. MetaboAnalyst 6.0: Towards a unified platform for metabolomics data processing, analysis and interpretation. *Nucleic Acids Res.* **52**, W398–W406 (2024).
96. Wahl, S. A., Dauner, M. & Wiechert, W. New tools for mass isotopomer data evaluation in (13)C flux analysis: Mass isotope correction, data consistency checking, and precursor relationships. *Biotechnol. Bioeng.* **85**, 259–268 (2004).
97. Evers, B. et al. Simultaneous Quantification of the Concentration and Carbon Isotopologue Distribution of Polar Metabolites in a Single Analysis by Gas Chromatography and Mass Spectrometry. *Anal. Chem.* **93**, 8248–8256 (2021).
98. Faubert, B., Tasdogan, A., Morrison, S. J., Mathews, T. P. & DeBerardinis, R. J. Stable isotope tracing to assess tumor metabolism in vivo. *Nat. Protoc.* **16**, 5123–5145 (2021).
99. Heinrich, P. et al. Correcting for natural isotope abundance and tracer impurity in MS-, MS/MS- and high-resolution-multiple-tracer-data from stable isotope labeling experiments with IsoCorrectoR. *Sci. Rep.* **8**, 17910 (2018).

Acknowledgements

We thank all members of the Inman and Golden labs for the feedback throughout the project, and the Amie Lund lab at the University of North Texas Denton for the use of a fluorescent microscope. We acknowledge the Prokai lab at UNT Health for advice regarding the use of GC-MS and Mark Pulse of Preclinical Services in the College of Pharmacy at UNT Health for use of his sample preparation equipment.

Author contributions

US and DMI conceptualized and designed the study. US performed experiments, interpreted the data, prepared the figures, and wrote an original draft. OY collected and analyzed data. KRS and TDG provided GC-MS expertise and instrumentation. KRS guided GC-MS experiment completion and data interpretation. EHS provided guidance and data interpretation across all isotope tracing experiments. DMI edited and finalized figures and the manuscript. DMI provided grant funding for the research. All authors provided feedback on the manuscript.

Funding

This project was supported by NIH grants EY026662 and EY036552 to DMI.

Declarations

Competing interests

The authors declare no competing interests.

Ethics approval

All animal procedures were reviewed and approved by the Institutional Animal Care and Use Committee (IACUC) at UNT Health under protocol number 2022-0026. The research was conducted in accordance with the guidelines set forth by the National Institutes of Health (NIH) Guide for the Care and Use of Laboratory Animals, ensuring humane care and ethical treatment of all animals used in this study.

Additional information

Supplementary Information The online version contains supplementary material available at https://doi.org/10.1038/s41598-026-50306-7.

Correspondence and requests for materials should be addressed to D.M.I.

Reprints and permissions information is available at www.nature.com/reprints.

Publisher's note Springer Nature remains neutral with regard to jurisdictional claims in published maps and institutional affiliations.

Open Access This article is licensed under a Creative Commons Attribution-NonCommercial-NoDerivatives 4.0 International License, which permits any non-commercial use, sharing, distribution and reproduction in any medium or format, as long as you give appropriate credit to the original author(s) and the source, provide a link to the Creative Commons licence, and indicate if you modified the licensed material. You do not have permission under this licence to share adapted material derived from this article or parts of it. The images or other third party material in this article are included in the article's Creative Commons licence, unless indicated otherwise in a credit line to the material. If material is not included in the article's Creative Commons licence and your intended use is not permitted by statutory regulation or exceeds the permitted use, you will need to obtain permission directly from the copyright holder. To view a copy of this licence, visit http://creativecommons.org/licenses/by-nc-nd/4.0/.

© The Author(s) 2026